論文 / 著書情報
Article / Book Information

論題(和文)	IMPACT ASSESSMENT OF 2023 CYCLONE MOCHA ON VEGETATION AND FLOOD USING REMOTE SENSING IMAGE ANALYSIS
Title(English)	IMPACT ASSESSMENT OF 2023 CYCLONE MOCHA ON VEGETATION AND FLOOD USING REMOTE SENSING IMAGE ANALYSIS
著者(和文)	Htut NAING THWIN, Hiroshi TAKAGI, Md. Rezuanul ISLAM
Authors(English)	Htut NAING THWIN, Hiroshi TAKAGI, Md. Rezuanul ISLAM
出典(和文)	Journal of JSCE, Vol. 13, No. 2,
Citation(English)	Journal of JSCE, Vol. 13, No. 2,
発行日 / Pub. date	2025, 10
権利情報 / Copyright	本著作物の著作権は土木学会に帰属します。 Copyright (c) 2025 Japan Society of Civil Engineers.

IMPACT ASSESSMENT OF 2023 CYCLONE MOCHA ON VEGETATION AND FLOOD USING REMOTE SENSING IMAGE ANALYSIS

Htut NAING THWIN[1], Hiroshi TAKAGI[2], Md. Rezuanul ISLAM[3]

[1]School of Environment and Society, Institute of Science Tokyo
(2-12-1, Ookayama, Meguro-ku, Tokyo 152-8550, Japan)
E-mail:htut.aa@m.titech.ac.jp (Corresponding Author)
[2]Member of JSCE, Professor, School of Environment and Society, Institute of Science Tokyo
(2-12-1, Ookayama, Meguro-ku, Tokyo 152-8550, Japan)
E-mail:takagi.h.ae@m.titech.ac.jp
[3]Department of Civil Engineering, Graduate School of Engineering, the University of Tokyo
(7-3-1 Hongō, Bunkyo City, Tokyo 113-8654, Japan)
E-mail:fahimislam@g.ecc.u-tokyo.ac.jp

Cyclone Mocha (2023), a Category 5 tropical cyclone, caused significant damage in Myanmar, particularly in Sittwe, the capital of Rakhine State. Despite its strong intensity and the death toll of at least 500 people, the event has not been fully investigated due to limited data availability, especially in remote rural areas. To address this information gap, remote sensing techniques using optical satellite imagery and synthetic aperture radar (SAR) imagery were employed to assess Mocha's impact on vegetation and inundation. Vegetation loss was analyzed using eVIIRS Global NDVI datasets, based on 10-day composite images of pre-, during-, and post-cyclone periods. The results revealed a small decrease in vegetation cover across over half of the study area, indicating a modest decline rather than complete destruction. In contrast, an increase in vegetation was also observed after the cyclone in areas away from the radius of maximum wind of the cyclone. SAR analysis suggested storm surge as the predominant factor contributing to the subsequent inundation. However, data from an inland town suggested the potential influence of riverine flooding and heavy precipitation as additional contributing factors. Using the CMEMS global model, the peak water level during the cyclone was estimated at 1.6 m at the closest point to the landfall location, marking the highest recorded level in the past 30 years. Furthermore, a local news photo showed visible inundation, likely caused by storm surge, reaching at least 0.5 m in downtown Sittwe.

Key Words : *cyclone mocha, remote sensing, vegetation index, inundation, forest damage*

1. INTRODUCTION

Cyclone Mocha, which struck Myanmar in May 2023, is considered one of the strongest tropical cyclones in the past decade, but the full extent of the disaster remains unclear, mainly due to difficulties in obtaining information caused by access limitations, ongoing conflict and communication challenges in the region[Note 1)]. Preliminary reports indicate that Mocha was among the strongest cyclones to impact the Bay of Bengal, reaching Category 5, and made landfall near Sittwe township in Rakhine state with wind speeds of 209 km/h[Note 2)], with an estimated 20-year return period[1)]. The cyclone is officially estimated to have killed at least 500 people and caused widespread destruction, especially in Rakhine State[Note 2)].

Despite the severity of Cyclone Mocha, comprehensive scientific studies detailing its impacts remain scarce, highlighting a critical research gap in understanding the full effects on affected communities and ecosystems. A similar situation was observed with Cyclone Nargis (2008), a Category 4-equivalent cyclone that resulted in over 138,000 fatalities. This disaster highlighted the importance of timely and accurate damage assessment for improving emergency response and recovery efforts in Myanmar[2)]. However, 15 years after Nargis, no significant improvements have been observed in the case of Mocha. Restrictions on humanitarian access and limited communication infrastructure have impeded data collection and analysis, making effective disaster response and resilience planning more challenging[Note 3)]. Military-imposed restrictions permit only routine pre-cyclone humanitarian activities while prohibiting any

large-scale cyclone-specific response. As a result, Tropical Cyclone Mocha caused widespread destruction, affecting an estimated 670,000 people[Note 3)].

Given these constraints, alternative damage assessment methods are essential. In this study, remote sensing techniques, including Synthetic Aperture Radar (SAR) and Normalized Difference Vegetation Index (NDVI) analysis, were used to estimate inundation and vegetation loss, which reflect inundation and wind impacts on ecological and agricultural systems, as proxies for total damage.

2. METHODOLOGY

(1) Target Area

This study focuses on the Rakhine region, particularly Sittwe, where Cyclone Mocha made landfall and three other densely populated cities—Yathedaung, Ponnagyun, and Mrauk-U (**Fig. 1**). According to AW3D data from the Japan Aerospace Exploration Agency (JAXA), this low-lying delta area has an average elevation of about 2 m.

Remote sensing techniques were utilized to assess damage for the total area of 20430 km² within the map extent boundary and in the most severely affected areas. Meteorological data was obtained from The International Best Track Archive for Climate Stewardship (IBTrACS) project.

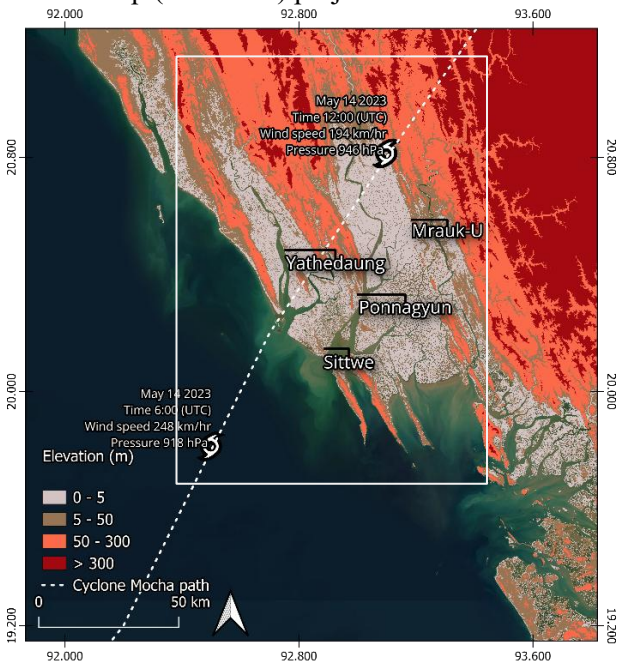

Fig. 1 Elevation map around the Rakhine coast in northwestern Myanmar, including the path of Mocha

(2) NDVI Analysis for Vegetation Area

The Global NDVI from EROS Visible Infrared Imaging Radiometer Suite (eVIIRS) with a 1-km resolution was utilized as the reference dataset due to its high temporal availability, providing imagery at every 10-day intervals[Note 4)]. The minimum NDVI value is −0.1999, and all NDVI values—typically ranging from –1.0 to 1.0—were scaled by a factor of 10,000, resulting in a range from –2000 to 10,000[Note 4)]. Three 10-day composite NDVI images (May 01–10, May 11-20, and May 21–31) were used to represent pre-, during-, and post-cyclone periods, respectively. NDVI values from the pre- and post-cyclone periods were compared, and the difference referred to as Differenced Normalized Difference Vegetation Index (DNDVI) was calculated.

DNDVI can be used to represent changes in vegetation coverage distribution and was calculated using the following formula[3)]:

$$DNDVI = NDVI_b - NDVI_a \quad (1)$$

where $NDVI_b$ and $NDVI_a$ represent pre- and post-cyclone period NDVI values, respectively. A positive DNDVI indicates a decrease in vegetation cover, and vice versa for negative values. DNDVI changes were classified into six levels according to intensity: significant decrease [10000 to 5000], moderate decrease [5000 to 2000], small decrease [2000 to 0], small increase [0 to −666], moderate increase [–666 to –1333], and significant increase [–1333 to –2000]. In the absence of ground truth data for DNDVI, the classification can be used for relative comparisons of vegetation change, but it is not appropriate for assessing vegetation health, specifically, the condition of vegetation remaining after the cyclone.

The Copernicus Global Dynamic Land Cover dataset provides a raster file in which each pixel represents a specific land cover type[4)]. Utilizing this dataset and the QGIS Raster Calculator, land cover was classified into forest, cropland, and settlement categories. A logical “AND” operation was applied during raster analysis to isolate vegetation damage by selecting pixels where the land cover matched the target class.

(3) SAR image Analysis for Flood Area

The Synthetic Aperture Radar (SAR) onboard the Advanced Land Observing Satellite (ALOS), operated by Japan Aerospace Exploration Agency (JAXA) provides 100-meter resolution satellite imagery every two weeks. This all-weather imaging capability is particularly valuable for rapid disaster assessment[5)].

To assess inundation, the average water index was calculated using thresholding on VV or VH Polarization, which correspond to satellite-transmitted and received signals, for SAR imagery using the methodology derived from Digital Earth Australia[Note 5)].

First, speckle noise was removed from the VV and

VH SAR images using a filtering technique to enhance image quality. Next, histograms representing the distribution of pixel values were analyzed. A bimodal threshold-based classification method was then applied, in which pixels with values below a defined threshold were identified as water and those above the threshold as land.

VH and VV polarization bands were analyzed across all available images captured during the cyclone period (May 9–15, 2023). The image with the highest average number of water pixels was selected to map the inundated area. Additionally, a photo obtained from local news sources was used to estimate flood depth, providing valuable insights into the on-ground condition, as will be discussed later.

(4) Sea Surface Elevation

To analyze sea surface height variations during Cyclone Mocha, data from the Global Ocean Physics Analysis and Forecast Model of Copernicus Marine Service[6] was processed to obtain hourly sea surface height above the geoid for a specific point on the coast of Sittwe shown in **Fig. 4**. Additionally, 30 years (1995–2025) of daily sea surface height data from the same source was used for historical comparison[6].

(5) Digital Elevation Model (DEM)

Elevation data above sea level was obtained from JAXA's AW3D dataset[7]. The study area is characterized by two notable topographic features: (1) high-elevation mountainous regions with long, narrow ridges and steep slopes, and (2) low-lying deltaic regions, particularly vulnerable to storm surges and flooding.

3. RESULTS

(1) Affected Vegetation

a) Vegetation changes

According to the results of the DNDVI analysis comparing before and after the cyclone within the mapped extent (**Figs. 2** and **3a**), the vegetation index decreased across an area of 15,608 km², accounting for 76.4% of the total vegetated area. This decline in vegetation can be attributed to the intense wind speed during landfall, which reached up to 54 m/s. Such high wind intensity is known to cause significant vegetation damage including the loss of up to 70% of leafy branches[8], leading to a reduction in canopy cover and lower NDVI values. Among the affected areas, 58 km² experienced a significant decrease in vegetation (DNDVI between 10,000 and 5,000), representing 0.3% of the mapped extent and indicating zones of severe vegetation loss. In contrast, the vegetation index increased (considering the combined area of small, moderate, and significant increases) across 4,820 km², representing 23% of the total mapped area. It can be expected that areas where the vegetation index increased are primarily located outside the radius of maximum wind, with minimal impact or natural vegetation occurred after cyclone landfall.

b) Vegetation changes by land cover type

Vegetation changes varied across different land cover types, revealing diverse patterns of impact. As shown in **Fig. 3(b)**, vegetation loss in settlement areas was relatively small, with a reduction of about 23 km². In cropland areas, about 2,480 km² experienced a decrease in vegetation index (ranging from small to significant decrease), while 1580 km² showed an increase (**Fig. 3c**). The most substantial decrease was observed in forested areas, where vegetation index declined across 7,600 km² (**Fig. 3d**). This is obvious because the forested land constitutes the largest share of trees and plants. In addition, the forested area in the study region is primarily located in the hills (~200 m), which likely exposed it to strong winds and contributed to the observed damage. Overall, 60% of the entire study area (20430 km² within the map extent) showed a slight decrease in the vegetation index, suggesting that vegetation was not entirely destroyed but rather experienced a modest decline. Notably, increases in vegetation index were observed across all land cover types. Although verification on the ground is needed, this was possibly due to successional vegetation, a process in which fast-growing and resilient pioneer species rapidly revegetate in disturbed areas[9].

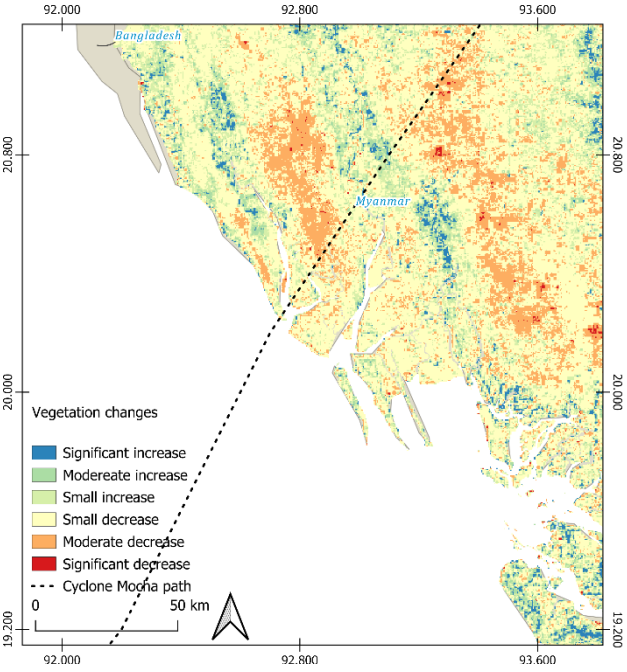

Fig. 2 Vegetation changes based on DNDVI

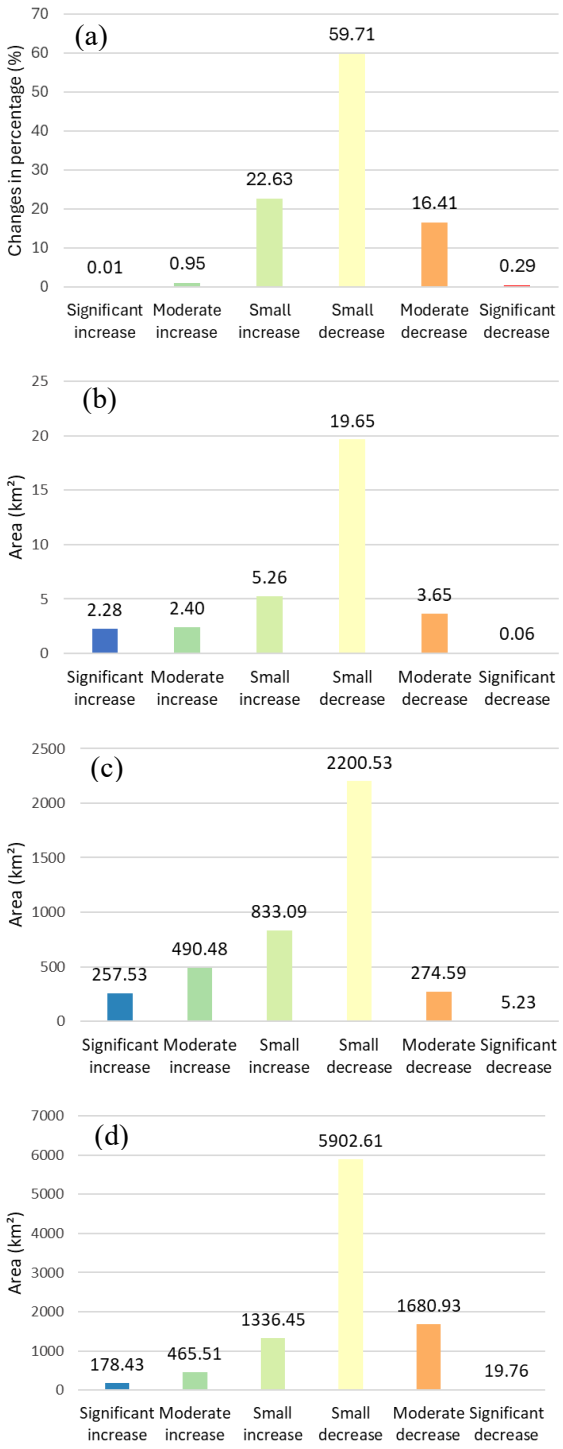

Fig. 3 Vegetation changes in: (a) entire study area (%), (b) settlement areas (km²), (c) cropland areas (km²), (d) forested areas (km²).

(2) Inundation and sea surface elevation

The total inundated area was about 4,000 km² (**Fig. 4**), encompassing 870 km² of cropland, 7 km² of settlement area, and 1,820 km² of forest area. The extensive flooding of croplands can be attributed to their low elevation, ranging from approximately 1 to 2 meters above sea level, making them highly susceptible to coastal inundation.

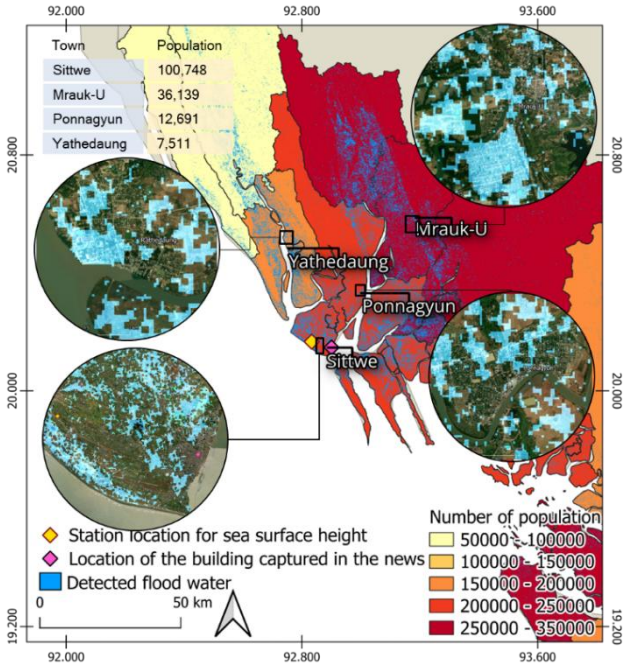

Fig. 4 Regional distribution of population from MIMU[Note 6)] and inundated areas, processed using ALOS SAR satellite imagery. The closer views highlighted by circles include four densely populated towns: Sittwe, Yathedaung, Ponnagyun, and Mrauk-U.

Flood impact was assessed in densely populated urban areas as shown in **Fig. 4**. In Sittwe, floodwater covered about 4 km², 20% of the total area of the city. In Mrauk-U, Ponnagyun, and Yathedaung, 3.5 km² (22%), 0.5 km² (28%), and 0.42 km² (39%) were flooded, respectively (**Fig. 5**). The total area for each city was defined according to township boundaries (**Fig. 5**). Although Sittwe and Mrauk-U have a similar total area, the impact on the population varied significantly. Sittwe, with a population of approximately 100,748, has nearly three times that of Mrauk-U, suggesting that the effects of flooding were likely most severe in Sittwe. However, when considering regional boundaries, Mrauk-U is situated within the most populous region, which also has the largest inundated areas, indicating a broader spatial impact of flooding in that region. This is followed by the region encompassing Sittwe and Ponnagyun, with the least affected region being where Yathedaung is located.

Being a coastal city, Sittwe is particularly vulnerable to the direct impact of storm surges. For example, the sea surface height at the station point near Sittwe in **Fig. 4** reached ~1.7 m on May 14, 2023, at 8:00. This height is the highest sea surface level recorded in the past 30 years (1995–2024). Considering the historical average sea surface height of 0.6 m as a baseline, the peak water level during the 2023 Cyclone was more than twice the average (**Fig. 6**).

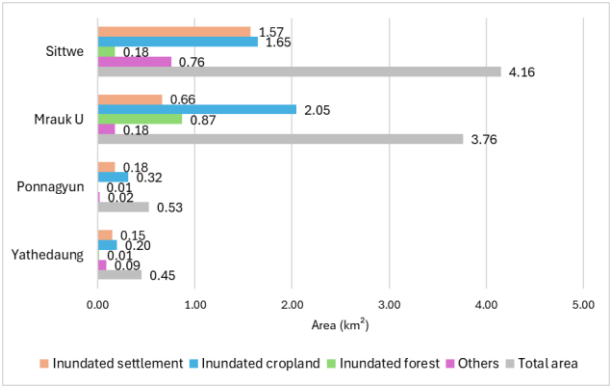

Fig. 5 Inundated areas per land cover type for each town. Note: Total area refers to the total land area of the town, not the total inundated area.

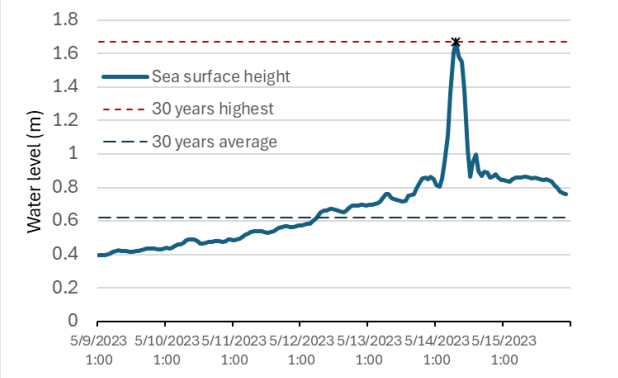

Fig. 6 Comparison of sea level during the cyclone, maximum sea level, and average water level for 30 years.

A local photograph (**Fig. 7**) taken in the downtown area of Sittwe, which was geo-referenced in Google Earth, proves evidence of significant inundation. A motorcycle was inundated by floodwaters approximately 0.5 m above the street level. The flood disaster hazard map of Kita City, Tokyo, indicates that even this level of flood depth makes pedestrian movement impossible[Note 7]. Balasbaneh et al. (2004) state that when flood depth reaches approximately 0.5 m, wooden structures—the most common building type in the study area—are caused around 20% damage, which increases to about 30% when floodwater exceeds 1.5 m[10]. Given the flat terrain with elevation 5 m above sea level (**Fig. 1**) and the increase in sea surface height adjacent to Sittwe, it is likely that storm surge was the primary cause of the subsequent flooding. Yathedaung and Ponnagyun are located near large rivers close to the coast (**Fig. 4**) and were likely affected by storm surges propagating upstream through these river channels. In contrast, Mrauk-U is further inland, around 60 km from the shoreline. The inundation of 3.5 km² in Mrauk-U is difficult to explain by storm surge alone, suggesting the combined influence of river flooding and heavy precipitation.

Fig. 7 Left: Estimation of flood inundation depth based on a photo taken on May 14, 2023 (Source: BBC Burmese), and Right: normal situation (Google Earth).

(3) Effects of elevation on vegetation damage and inundation

An analysis of 17,075 randomly sampled data points (0.1% of the total; **Fig. 8**) examines the relationship between elevation, DNDVI, and inundation. Inundation predominantly occurs at lower elevations, while non-inundated areas are distributed across a wider range of elevations. DNDVI values in inundated areas vary widely, indicating flooded areas can experience both vegetation damage and recovery. The non-inundated areas, mostly highlands, also have a wide range of DNDVI values.

A hexbin visualization of all data points (**Fig. 9**) highlights the density of observations, revealing that the highest concentration of data points is found at lower elevations, where DNDVI variability is greatest. This suggests these areas are susceptible not only to vegetation damage but also to vegetation regrowth, which warrants further investigation. The accompanying histogram indicates that the distribution of DNDVI is close to a normal distribution. For the areas above 1500m elevation, the DNDVI range is narrow (–500 to 1500), and the values are mostly positive, indicating minimal vegetation loss.

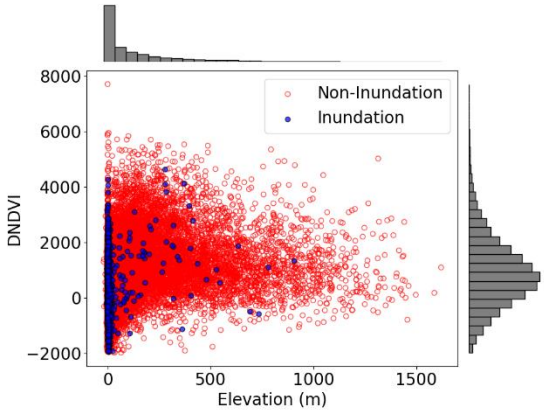

Fig. 8 A random sample scatterplot of DNDVI, elevation, and inundation status

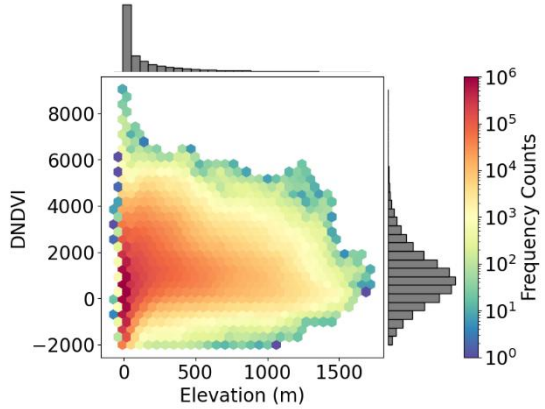

Fig. 9 Hexbin scatterplot of DNDVI and elevation with histograms

4. CONCLUSIONS

In this study, the impact of Cyclone Mocha on vegetation loss and inundation was assessed using remote sensing. The cyclone damage was estimated by analyzing changes in vegetation index, NDVI, and DNDVI. Overall, NDVI decreased across 15,608 km², representing 76% of the total area. The most severe vegetation loss was observed in forested regions, affecting 7,600 km². At lower elevations, DNDVI variability is the greatest, with a broad range of values, suggesting, while the cyclone caused a moderate reduction in vegetation, this elevation range also has the highest potential for vegetation recovery.

Regarding flooding, croplands were particularly affected, with 870 km² out of the 4,000 km² total inundated area. The sea level rise caused by Cyclone Mocha was the highest in the past 30 years, highlighting the intensity of the storm. Social media reports estimated the storm surge height to be about 0.5 m above the street level in downtown Sittwe, which is deep enough to damage wooden structures.

The present study has encountered unmanageable limitations, the most critical being the absence of ground truth data. The ongoing political unrest and civil war have made conducting field surveys or obtaining data from authorities virtually impossible. Under these circumstances, remote sensing approaches were deemed to provide a valuable initial assessment. However, remote sensing inherently lacks the contextual understanding that on-ground assessments provide. For instance, it is challenging to differentiate between temporary vegetation loss and long-term degradation using satellite data alone. While this study focuses on Cyclone Mocha, the approach holds promise for broader application in future research. This includes validation against historical cyclones where ground truth data exists, which could improve damage estimation in disaster-affected zones that are difficult to access.

ACKNOWLEDGMENTS: We extend our gratitude to the Kubota Fund for its generous scholarship support provided to the first author.

NOTES

Note 1) United Nations Myanmar, https://myanmar.un.org/en/234994-iom-myanmar-cyclone-mocha-response-situation-report-2-may-25-2023

Note 2) The Mainichi, https://mainichi.jp/english/articles/20230520/p2g/00m/0in/007000c.

Note 3) Médecins Sans Frontières, https://www.msf.org/cyclone-mocha-aid-efforts-severely-hampered-new-,restrictions

Note 4) EROS Visible Infrared Imaging Radiometer Suite (eVIIRS). 10.5066/P9QOEFNP

Note 5) Digital Earth Australia, https://knowledge.dea.ga.gov.au/notebooks/Real_world_examples/Radar_water_detection/

Note 6) Myanmar Information Management Unit (MIMU), https://themimu.info/

Note 7) Kita City disaster prevention portal https://bosai-portal.city.kita.tokyo.jp/assets/r5arakawamape.pdf

REFERENCES

1) Bhardwaj, P., Singh, O. & Yadav, R.B.S. Probabilistic assessment of tropical cyclones' extreme wind speed in the Bay of Bengal: implications for future cyclonic hazard. Nat Hazards 101, 275–295 (2020).
2) Fritz, Hermann & Blount, Christopher & Thwin, Swe & Thu, Moe & Chan, Nyein. (2009). Cyclone Nargis storm surge in Myanmar. Nature Geoscience. 2. 448-449.
3) Lu, L.; Wu, C.; Di, L. Exploring the Spatial Characteristics of Typhoon-Induced Vegetation Damages in the Southeast Coastal Area of China from 2000 to 2018. Remote Sens. 2020, 12, 1692.
4) European Union's Copernicus Land Monitoring Service information, https://land.copernicus.eu/en/products/global-dynamic-land-cover/copernicus-global-land-service-land-cover-100m-collection-3-epoch-2019-globe
5) Advanced Land Observation Satellite Project, https://www.eorc.jaxa.jp/ALOS/en/dataset/palsar2_l22_e
6) Copernicus Marine Service, https://data.marine.copernicus.eu/product/GLOBAL_MULTIYEAR_PHY_001_030/
7) T. Tadono, H. Ishida, F. Oda, S. Naito, K. Minakawa, and H. Iwamoto, "Precise Global DEM Generation by ALOS PRISM", ISPRS, Remote Sensing and Spatial Information Sciences, Vol.II-4, pp.71-76, 2014.
8) Feuerstein, Bernold & Groenemeijer, Pieter & Dirksen, Erik & Hubrig, Martin & Holzer, Alois & Dotzek, Nikolai. (2011). Towards an improved wind speed scale and damage description adapted for Central Europe. Atmospheric Research - ATMOS RES. 100. 547-564.
9) Elmqvist, Thomas & Wall, Maria & Berggren, Anna-Lena & Blix Germundsson, Lisa & Fritoff, Asa & Rinman, Ulrika. (2001). Tropical Forest Reorganization after Cyclone and Fire Disturbance in Samoa: Remnant Trees as Biological Legacies. Conservation Ecology. 5.
10) A T Balasbaneh et al 2020 IOP Conf. Ser.: Earth Environ. Sci. 476 012004

(Received February 4, 2025)
(Accepted May 15, 2025)